Study of the two-phase liquid loading phenomenon by applying CFD techniques

Joaquín Vieiro[1], Miguel Asuaje[2] and Geanette Polanco[3]
[1]Department of Energy Conversion and Transport. Simon Bolivar University, Caracas, Venezuela, 02-35541@usb.ve
[2]Department of Energy Conversion and Transport. Simon Bolivar University, Caracas, Venezuela, asuajem@usb.ve
[3]Department of Mechanics. Simon Bolivar University, Caracas, Venezuela, gpolanco@usb.ve

ABSTRACT
In order to understand the liquid loading phenomenon, 2D (axisymmetric) numerical simulations were performed. This phenomenon appears when the gas velocity reduces to a value below the critical speed of drop extraction in two-phase production wells, and as consequence liquid is accumulated in the tubing, increasing the pressure drop and reducing the flow rate within the tube. Simulations were made using air-water as working fluids over a vertical pipe of 4 meters long through a commercial package of CFD. Comparison between the simulation results and the experimental data available in the literature shows a good capability of homogeneous models to predict the flow characteristics for a given velocity range close to the critical gas velocity; over 100% of this parameter the model significantly overestimates the pressure drop.

Key words: Upward annular flow; homogenous model; liquid loading.

NOMENCLATURE

d	Inner diameter of the pipe
Fr	Froude number
g	Acceleration of gravity
L	Length
LVF	Liquid volume fraction
P	Pressure
Rc	Cutoff radius
r	Radial coordinate
t	Time
Vs	Superficial velocity
w	Axial velocity
y^+	Dimensionless wall distance
z	Axial coordinate

GREEK SYMBOLS:

δ	Film thickness
μ	Viscosity
ρ	Density

SUBSCRIPTS

g Gas phase

l Liquid phase

1. INTRODUCTION

Early in a gas well life, the energy needed to extract the liquid out of the well comes from the gas produced. Over time, the flow energy is reduced until a critical point is reached, in which, the gas velocity is just sufficient to raise the liquid from the bottom of the well. From this point, any reduction in gas speed will result in accumulation or liquid load on the base of the well. This accumulation causes a rising in hydrostatic pressure, which increases the pressure difference required to maintain the level of production. Without implementation of an extraction method for reducing fluid level or pressure drop in the well, the production is reduced and it eventually ceases [1].

Currently, to control this phenomenon and to assure the flow, there are some liquid extraction methods, such as, mechanical pumping, compression of gas, reduction of tubing diameter, application of surfactants, among others. These extraction techniques generally require capital investment and significant operating costs.

Understanding the two-phase flow in gas wells is vital to predict the conditions, to prevent damage or loss of reservoirs. This research will focus on describing and explaining the behavior of two-phase flow velocities near the critical speed of extraction in vertical pipes. A Computational Fluid Dynamics (CFD) commercial code called ANSYS® CFX™ 13.0 was employed for this purpose. This powerful tool has been validated in numerous applications in various areas of industry. Its application allows a detailed picture of flow patterns, phase velocity, pressure gradients, etc. in various sections of the well and various stages of its life.

2. REVIEW

There have been numerous theoretical and experimental studies to describe and predict this phenomenon. One of these is the work done by Turner *et al.* [2] who developed models of droplets and film extraction, in order to estimate the minimal speed of gas for liquid extraction. They compared their results with a database of well data (most of them with wellhead pressure greater than). They concluded that the particle model define more adequately the critical velocity of liquid extraction. The Turner's droplet model consists in a force balance on a drop in a gas stream flowing vertically upwards, where the weight is acting downward and the interfacial drag force acts upward. The critical speed is obtained when the drag forces and weight are equal. Turner assumed that the droplet is perfectly spherical and rigid. The droplet diameter was calculated considering a Weber number equal to 30 [3]. They introduced a correction factor of 20% to improve their results in order to fit the field data. This model predicts a critical velocity value of for air-water flow.

Coleman *et al.* [4] developed a model similar to Turner *et al*. [2], with the difference that it was not necessary to apply the correction factor of 20% because the original result was adjusted to field data with wellhead pressure of less than . The air-water critical velocity for this model was.

Han [5] performed CFD simulations using Fluent® 6.18 software, to investigate the mechanism of liquid entrainment in upward annular flow. Initially, simulations in simplified 2D domain of a circular pipe of length and radius were performed to visualize the flow characteristics in the gas core. He developed steady state simulations using renormalization group $k - \varepsilon$ turbulence model and improved wall treatment. The two-phase interface was

formed as a corrugated wall with constant speed according to the model developed by Zhu [6]. Han [5] also developed 2D two-phase flow air-water simulations on nonpermanent regime, applying the renormalization group model and the improved wall treatment. Interface reconstruction was done by applying the volume of fluid (VOF) method. He reproduced annular flow pattern using two regions of fluid access: gas enters the central part of the section, and annular inlet of water from the pipe wall to the border of the gas region. Due to computational limitations, first-order schemes were used in solving equations. A value of 10^{-3} was selected as convergence criteria of all residuals. He obtained that the details of the drag mechanism are well described by the model used in the simulations. The flow patterns were similar when compare with experimental work.

Van 't Westende *et al.* [7] studied the influence of droplets on the occurrence of liquid backflow on air-water two-phase flow in an long vertical Plexiglas tube. The experimental assembly had a gas entrance arranged at the lower end of the pipe, a liquid entrance at one meter above bottom and the top end open to the atmosphere. At the bottom of the pipe a waterlock used in cases of liquid backflow was present. Annular-mist and annular-churn flow patterns were reproduced. They measure pressure drop, wave velocity, gas velocity, in addition to diameter distribution, entrainment and speed of droplets, among others. They observed that, for superficial velocities of gas and liquid of and , respectively, there was no large amount of droplets with velocities close to zero (almost all moved upward at approximately), and those drops were not very large, unlike the proposed by Turner *et al*. [2] were the droplets have a diameter of . They said that the droplets unlikely cause directly liquid loading. However, the drops could indirectly produce backflow presence, since they reduce the gas speed near the gas-liquid interface, causing reduction of interfacial shear, which can result in film instability. They recognized the point of minimum pressure drop when the densimetric Froude number is equal to unity, i.e., the superficial gas velocity is .

Parvareh *et al.* [8] implemented simulations in permanent regime using Fluent 6.2, to reproduce flow patterns in horizontal and vertical pipe. They used a 3D tetrahedral mesh with separate fluid inlets. The boundary conditions applied were: velocity inlets, atmospheric static pressure outlet and non-slip smooth walls. They took into account the effects of gravity. Initially, the domain was completely filled with water. The resolution was carried out using a finite volume method discretization with a combination of the PISO algorithm and a second order upwind scheme with time steps of $2\times10^{-3}s$. They reproduced wavy stratified, plug and annular flow in horizontal pipes, and slug and annular flow in a vertical pipe. To validate the results, they were compared with experimental data. Same flow patterns for both the experiment and simulations were obtained.

3. MODELING PROCESS

In order to promote phase separation, separated entries and homogeneous model was chosen. This model is recommended for cases where the fluids are completely segregated and there is a clearly defined interface between them. Water was selected as liquid phase, because this phase requires higher gas velocities for extraction [2]. The gas phase used was air at constant properties. There are some experimental data to validate with these two fluids. Both phases are modeled as continuous fluids. Since there is an important area adjacent to the walls, the built in SST turbulence model is applied. Finally, the boundary conditions were defined as mass flow rate inlets, atmospheric static pressure outlet and non-slip smooth wall.

3.1 STUDIED AREA

The gas and liquid superficial velocities were selected to be located in the annular flow region near the transition with churn flow. Experimentally, this region includes the $Fr_g = 1$ line, variable defined as the ratio of inertial forces and flotation density difference, as shown in Eqn. (1).

$$Fr_g = \frac{v_s^2 g}{g \cdot d} \frac{\rho_g}{\rho_l - \rho_g} \tag{1}$$

Study intervals are shown in table 1.

Table 1. Study intervals of superficial velocities

	Min	Max
Gas superficial velocity Vs_g (m/s)	12	48
Liquid superficial velocity, Vs_l (m/s)	0.02	0.08

3.2 GOVERNING EQUATIONS

The fundamental equations describing the incompressible Newtonian flow without heat or mass transfer and sources are:

Continuity equation. Expresses the principle of conservation of mass applied to a differential element. It is given by Eqn. (2).

$$\frac{\partial \boldsymbol{u}_k}{\partial x_k} = 0 \tag{2}$$

Momentum equations. Represent a force balance on a fluid element. These equations are given by Eqn. (3).

$$\rho \frac{\partial \boldsymbol{uj}}{\partial t} + \rho u_k \frac{\partial u_j}{\partial x_k} = -\frac{\partial p}{\partial x_j} + \mu \frac{\partial^2 u_j}{\partial x_i \partial x_i} + \rho g \tag{3}$$

Due to the simplifications made in this study, the energy and equations of state are outside the scope of this investigation.

3.3 GEOMETRY AND BOUNDARY CONDITIONS

To compare with the experiment of Van't Westende *et al*. [7], it is necessary to create a domain with the following characteristics:

- Vertical straight pipe of 4*m* (instead of 12*m* used in flow test facility) and an 0.0508*m* inner diameter circular cross section.
- Separated inlets: air at the lower end, and water through a wall section.
- Output at the top.

Since the problem has axial symmetry on the geometry and boundary conditions, the results

is expected to be axisymmetric and therefore, it is redundant to solve the entire pipe (Figure 1a) or even a half pipe (Figure 1b). Since 2D domains (Figure 1c) are not supported in ANSYS CFX 13.0, an axisymmetric approach was chosen for the simulations. If any actual condition does not fulfill the condition of axisymmetry, including the acceleration of gravity alignment with the tube axis, then the problem cannot be modeled this way.

An axisymmetric geometry was selected in the form of wedge of 5° as shown in Figure 1(d). The domain length is about 60 pipe diameters.

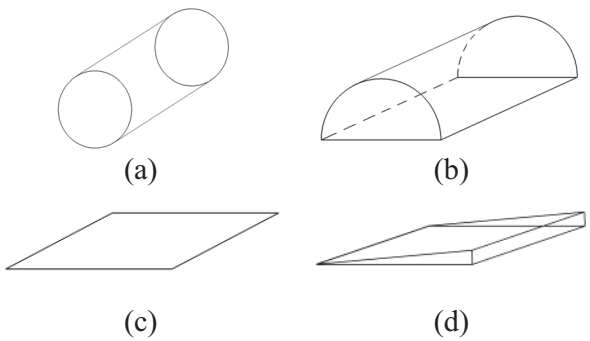

Figure 1. Ways of modeling the geometry: (a) full three-dimensional, (b) symmetrical three-dimensional, (c) plane, (d) axisymmetric

3.4 MESH

The domain regularity makes obvious the advantages of using a structured mesh in solving the problem. Thus, trapezoidal prismatic elements form the greater part of the mesh. The remainder being composed of triangular prismatic elements especially the axisymmetric axis which forms the apex of the triangle.

Triangular prism type elements reduce the quality of the mesh, so it raises the possibility of eliminating these elements by making a small cut on a radius on the geometry as shown in Figure 2.

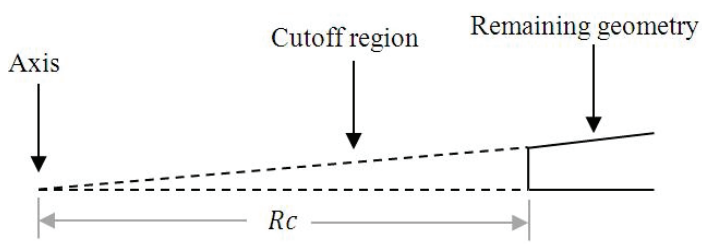

Figure 2. Cut made in the geometry

The mesh elements were made smaller in the zone near the tube wall and larger at the center; meanwhile the elements along the axis were uniformly distributed. In the angular direction there are only two nodes.

In order to verify the independence of the results in function of the mesh refinement, a series of six meshes was generated. The characteristics of the meshes are shown in Table 2.

Table 2. Meshes characteristics

	Nodes	Elements
1	299092	146250
2	901842	444500
3	81648	39100
4	662538	326400
5	1564398	774200
6	3053088	1515800

COMPUTATIONAL ARRANGEMENT SUMMARY

The following table summarizes the conditions applied:

Table 3. Summary of conditions

Gas phase	Air at 25ºC (continuous)
Liquid phase	Water (continuous)
Multiphase flow	Homogeneous
Turbulence model	SST
Drag model	Mixture
Buoyancy model	Density difference
Heat transfer	No

Gas inlet	Mass flow
Liquid inlet	Mass flow
Outlet	Static pressure
Wall	Smooth, no slip
Symmetry planes	Symmetry
Regime	Permanent
Discretization scheme	Second order
Turbulence	High resolution

The results of the simulations made with conditions in Table 3 and meshes in Table 2 and those made using 3-D symmetric mesh of 180° as shown in Figure 1(b) with number of nodes between 83664 and 4644708 nodes were used to perform a validation study of the

axisymmetric meshes, specifically using the liquid and gas superficial velocities values of Vs_l = 0.04 m/s and Vs_g = 29 m/s, respectively.

It was selected the result of pressure drop of the denser axisymmetric mesh (Mesh 6) and compared with lower density for assessing the effectiveness of the discretization, thus evaluating the cost in the number of nodes. In single-phase simulations, meshes 4 and 5 were within the range of 1% relative to the reference, however, considering that the mesh 4 has fewer elements, that mesh was selected. The same criterion was applied for two-phase flow using a range of 2%; here the difference was also obtained for the mesh 4. The selected mesh (Mesh 4) has a maximum value of y^+ equals 4. The pressure drop curve as a function of the number of nodes is shown in Figure 3. The first 2 points of 3D meshes are above 1000 *Pa*/*m*. Both axisymmetric and 3D meshes show an asymptotic trend.

The numerical discretization uncertainty based on GCI [9] evaluated for the mesh 4 along with 2 and 3 is 1,5%.

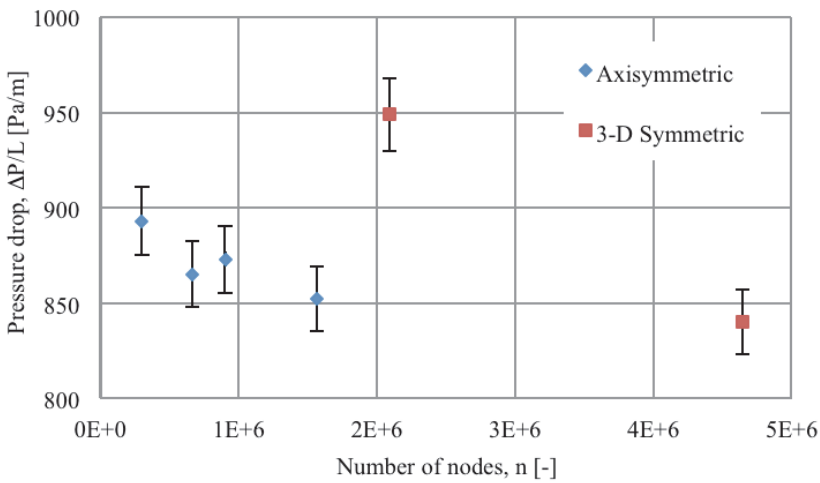

Figure 3. Pressure drop in function of the number of nodes for mesh independence study in two-phase flow simulations.

4. RESULTS

All simulations were terminated when the residuals of velocity reached 10^{-4} and imbalances of mass were less than 5%, except for the simulations with Froude number less than unity, which required softening the convergence criterion for velocity residuals to 5×10^{-4}.

4.1 PRESSURE DROP AS A FUNCTION OF SUPERFICIAL VELOCITY

The pressure drops given by the simulations with some of the measurements of Van't Westende *et al*. [7] are shown in Figure 4.

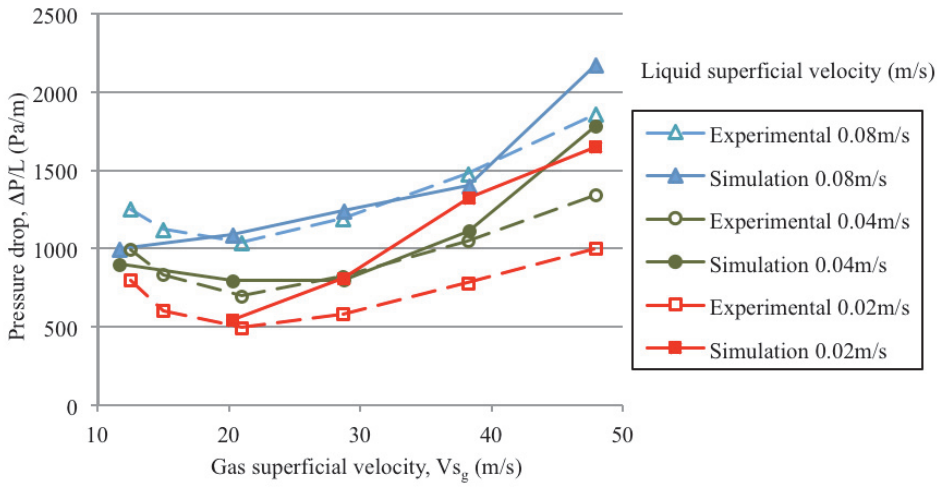

Figure 4. Pressure drop for various superficial velocities of gas a liquid

It can be seen in the curves of superficial velocity 0.04 *m/s* and 0.08 *m/s*, that the results are consistent with the experimental values of Van't Westende *et al*. (2007) until superficial gas velocities are close to 40 *m/s*. From there, deviations from the model grow significantly. The curve $Vs_l = 0.02$ *m/s* shows important overprediction in almost all points of study.

Curves of $Vs_l = 0.02$ *m/s* and $Vs_l = 0.08$ *m/s* reproduce the growing trend of pressure drop with increasing superficial gas velocity, without being able to capture the presence of a minimum value in critical Froude condition. However, the model reproduced point of minimum pressure drop for $Vs_l = 0.04$ *m/s*, which corresponds to a value of Fr_g close to 1.3 ($Vs_l = 20$ *m/s*). It was observed that the drag cannot elevate the film as in cases with higher gas velocity. This is attributed to an effect on the film that is not reproduced by the simulations: at points with Fr_g near and below 1, the film grows in the vicinity of the liquid inlet and is carried upward diffusely. This reduces the interfacial shear, giving lower pressure drops, as found in Figure 4.

In contrast to what experimental studies [7] reported for gas superficial velocities of 12 *m*/s, speed below the fluid return point, there was no liquid in the zone between the gas and liquid inlets.

Matching the pressure drop by itself does not guarantee that simulations are describing the actual physical phenomenon, so it is also studied the distribution of phases in the domain.

4.2 VELOCITY PROFILES AND LIQUID VOLUME FRACTION

All velocity profiles show a common feature: two distinct growing zones, first, adjacent to the wall in the area with high liquid volume fraction (defined as the ratio of the volume occupied by the liquid phase in a cell to the volume of the same cell), and the second one in the region where the liquid fraction is close or equals to zero. Figure 5 shows a velocity profile and the volume fraction of liquid, both for z = 3.5 *m* for the simulation with $Vs_l = 0.04$ *m/s*, $Vs_g = 29$ *m/s*.

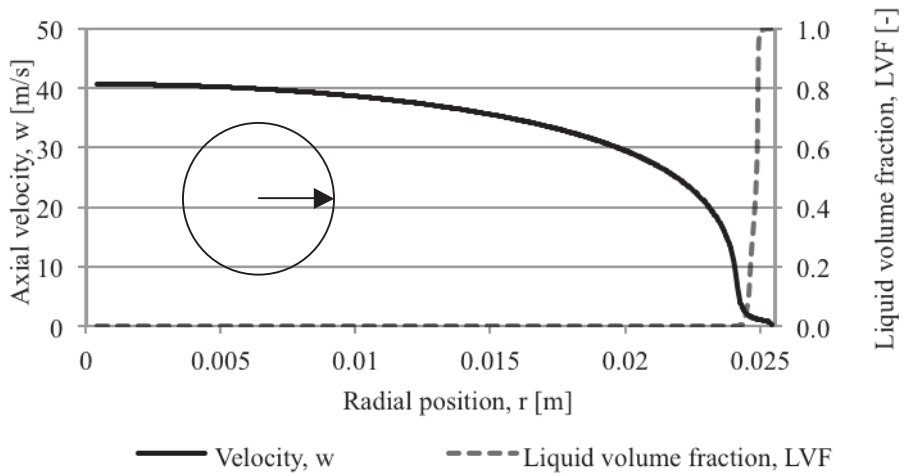

Figure 5. Velocity profile and *LVF* for Vs_g 29 *m*/s, Vs_l 0.04 *m*/s

The axial velocity profile has the characteristic shape of turbulent flow in pipes in the area of *LVF* = 0. Close to the wall where the *LVF* is nonzero, Figure 5 shows that the value of the axial velocity is dramatically reduced. Figure 6 presents a more detailed view of the behavior of *w* and *LVF* near to the wall.

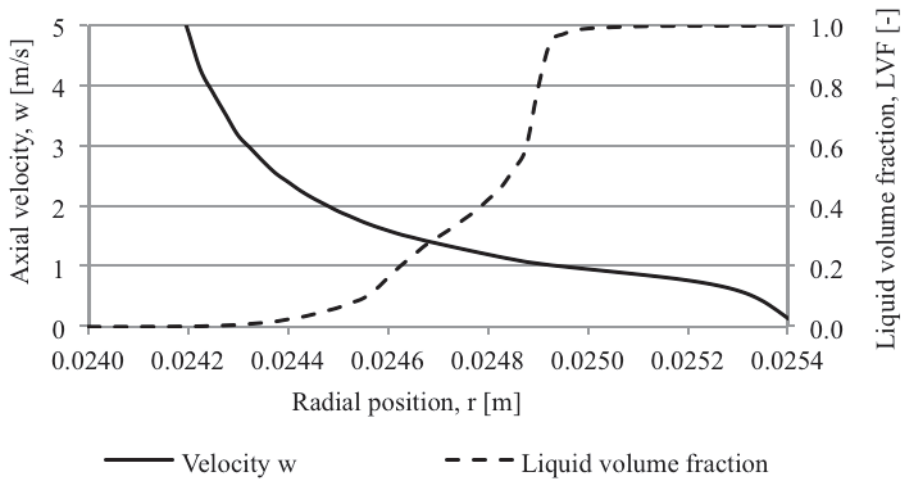

Figure 6. Detailed view of near-wall behavior

Note a concavity change point within the rapid reduction zone of *LVF* near to the value *LVF* = 0.5. That point was selected as a criterion for interface location.

4.3 FILM THICKNESS

The liquid phase was always near to the wall, where the liquid volume fraction reaches its maximum value. Since a non-free surface model was applied, the interface between the fluids is not defined. The location of a concavity change of the axial velocity profiles, as described above, is taken as the interface between the fluids. This point comes close to *LVF* = 0.5. To identify the sensitivity of film thickness depending on *LVF*, a comparison of thickness values for *LVF* = 0.3, 0.5 and 0.7 with $Vs_l = 0.8\ m/s$ is presented. The film thickness is taken as the average value between z = 3.40 *m* and z = 3.60 *m* taking 20 equally spaced measurement points. The results show that the sensitivity varies with the superficial gas velocity as shown in Figure 7.

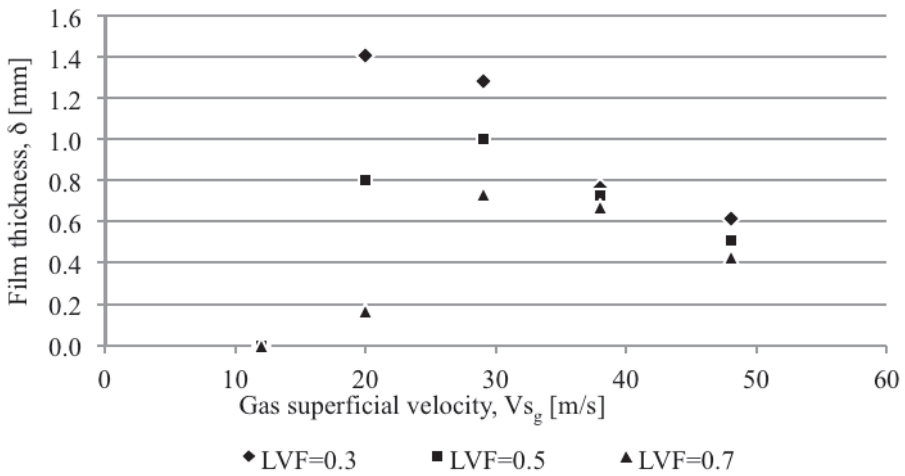

Figure 7. Sensitivity of the film thickness criterion

Points for *LVF* = 0.5 and 0.7 show the same tendency in the studied range, which is that the fill thickness decreases when gas superficial velocity increases as expected. However, the criterion for *LVF* = 0.3 behaves differently; in fact, this criterion oversized the film thickness since this includes the mist next to the film.

Table 4 shows images of different films obtained in the simulations. These images were taken at positions where the film has the average thickness reported above.

The table down shows that the film reduces its thickness as the superficial gas velocity increase or liquid superficial velocity reduces until the liquid reaches $Fr_g = 1$, as shown [7], [10] and [11]. For a further reduction of the value of Fr_g, the film disappears for the three criteria depending on the interface *LVF*. The qualitative behavior of the liquid film corresponds to the physical interaction determined by the above described drag.

Table 4. Liquid volume fraction in average film sections for different conditions

$Vs_g(m/s)$ \ $Vs_l(m/s)$	0.02	0.04	0.08
12 ($Fr_g = 0.4$)			
20 ($Fr_g = 1.0$)			
29 ($Fr_g = 1.9$)			
38 ($Fr_g = 3.4$)			
48 ($Fr_g = 5.4$)			
Scale		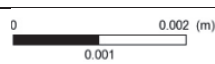	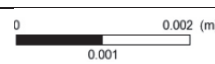
LVF	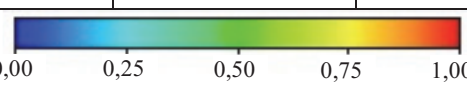		

5. CONCLUSIONS

After finishing this work, a series of conclusions can be drawn as follows:

Applicability of axisymmetric mesh in the simulation of annular two-phase flow in vertical pipes was demonstrated.

Homogeneous model and separated fluids inlets yielded a good approximation to the solution when compared with experimental results for densimetric Froude numbers between 1 and 3.5. The numerical modeling fails to reproduce the pressure drop for cases evaluated in the lower and upper end of the superficial gas velocity range selected (12 *m*/*s* and 48 *m*/*s*), which correspond to gas Froude values of 0.4 and 5.4, respectively. Nevertheless, it is possible to capture the physics of the film presence for cases of the larger than $Fr_g = 5.4$. This situation remarks that a criterion based only in the pressure drop evaluation is not strong enough to discuss about the full applicability of numerical techniques to this type of problems.

Homogeneous velocity profiles adequately describe the area in which the liquid volume fraction equals zero.

Increasing superficial gas velocity, improves the definition of the film, and also increases deviations in the results of pressure drop.

ACKNOWLEDGMENTS

This research was made possible by financial support of PETROBRAS.

REFERENCES

[1] Lea, J. F., Nickens, H. V. and Wells, M. R., Gas well deliquification, Second Edition, Gulf Professional Publishing, 2008.

[2] Turner, R. G., Hubbard, M. G. and Dukler, A. E., Analysis and Prediction of Minimum Flow Rates for the Continuous Removal of Liquid from Gas Wells, *Journal of Petroleum Technology*, 1969, 21 (11), 1475-1482.

[3] Hinze, J. O., Fundamentals of the Hydrodynamic Mechanism of Splitting in Dispersion Processes, *AIChE Journal*, 1955, 1 (30), 289-295.

[4] Coleman, S. B., Clay, H. B., McCurdy, D. G. and Norris, L. H. III, The Blowdown-Limit Model, *Journal of Petroleum Technology*, 1991, 43 (3), 339-343.

[5] Han, H., A study of entrainment in two-phase upward cocurrent annular flow in a vertical tube, Ph. D. Thesis, University of Saskatchewan, 2005.

[6] Zhu, Z. F., A Study of the Interfacial Features of Gas-Liquid Annular Two-Phase, M. Sc. Thesis, University of Saskatchewan, 2004.

[7] Van 't Westende, J. M. C., Kemp, H. K., Belt, R. J., Portela, L. M., Mudde, R. F. and Oliemans, R. V. A., On the role of droplets in cocurrent annular and churn-annular pipe flow, *International Journal of Multiphase Flow*, 2007, 33, 595–615.

[8] Parvareh, A., Rahimi, A., Alizadehdakhel, A. and Alsairafi, A. A., CFD and ERT investigations on two-phase flow regimes in vertical and horizontal tubes, *International Communications in Heat and Mass Transfer*, 2010, 37 (3), 304-311.

[9] Celik, I. B., Ghia, U., Roache, P. J. and Freitas, C. J., Procedure for Estimation and Reporting of Uncertainty Due to Discretization in CFD Applications, *Journal of Fluids Engineering*, 2008, 130 (7).

[10] Zabaras, G., Dukler, A. E. and Moalem-Maron, D., Vertical upward cocurrent gas–liquid annular flow, *AIChE Journal*, 1986, 32 (5) 829–843.

[11] Fore, L. B., and Dukler, A. E., Droplet deposition and momentum transfer in annular flow, *American Institute of Chemical Engineers Journal*, 1995, 41 (9), 2040–2047.